Self-Navigated Isotropic Three-Dimensional Cardiac T$_2$ Mapping

Ruud B. van Heeswijk,[1,2]* Davide Piccini,[1,2,3] Hélène Feliciano,[1,2] Roger Hullin,[4] Juerg Schwitter,[5] and Matthias Stuber[1,2]

Purpose: To implement and characterize an isotropic three-dimensional cardiac T$_2$ mapping technique.
Methods: A self-navigated three-dimensional radial segmented balanced steady-state free precession pulse sequence with an isotropic 1.7-mm spatial resolution was implemented at 3T with a variable T$_2$ preparation module. Bloch equation and Monte Carlo simulations were performed to determine the influence of the heart rate, B$_1$ inhomogeneity and noise on the T$_2$ fitting accuracy. In a phantom study, the accuracy of the pulse sequence was studied through comparison with a gold-standard spin-echo T$_2$ mapping method. The robustness and homogeneity of the technique were ascertained in a study of 10 healthy adult human volunteers, while first results obtained in patients are reported.
Results: The numerical simulations demonstrated that the heart rate and B$_1$ inhomogeneity cause only minor deviations in the T$_2$ fitting, whereas the phantom study showed good agreement of the technique with the gold standard. The volunteer study demonstrated an average myocardial T$_2$ of 40.5 ± 3.3 ms and a $<15\%$ T$_2$ gradient in the base-apex and anterior-inferior direction. In three patients, elevated T$_2$ values were measured in regions with expected edema.
Conclusion: This respiratory self-navigated isotropic three-dimensional technique allows for accurate and robust in vitro and in vivo T$_2$ quantification. **Magn Reson Med 000:000–000, 2014. © 2014 Wiley Periodicals, Inc.**

Key words: T$_2$ mapping; myocardium; self-navigation; 3D; isotropic

INTRODUCTION

Various pathological conditions are accompanied by edema, which is an increase in the relative amount of free water (1), and its presence in a tissue results in an increase in the T$_2$ relaxation time. Magnetic resonance imaging (MRI) can thus be used to detect edema, both qualitatively through T$_2$-weighted imaging (2) and quantitatively through T$_2$ mapping. In the case of cardiovascular disease, T$_2$ mapping with a variable T$_2$ preparation module (T$_2$Prep) (3) allows for the quantification of edema in the presence of cardiac and respiratory motion. Recently, such T$_2$ mapping has been applied to assess edema in patients with myocardial infarction (4,5), inflammatory cardiomyopathy (6), and heart transplant rejection (7,8). However, these T$_2$ maps are typically acquired as one or several two-dimensional (2D) slices, while the underlying pathology often has a complex three-dimensional (3D) structure. In addition, a 3D approach will sample considerably more myocardial tissue per unit time than a 2D approach, and might thus increase the precision of T$_2$ determination.

An isotropic 3D acquisition is therefore highly desirable, but significant time constraints apply in a clinical setting as the acquisition has to be repeated at least three times with incremental T$_2$Prep echo time (TE$_{T2Prep}$). Moreover, a delay of several heartbeats between acquisitions is often necessary to allow for magnetization recovery and to avoid artifacts due to heart rate variations (4). As a result, the scan duration of a T$_2$ map can easily be 6–12 times as long as that for the acquisition of a regular image. Given that a conventional navigator-gated 3D whole-heart acquisition takes on the order of 14–18 min (9), this would theoretically result in a total acquisition time of well over an hour.

The logical step would therefore be to exploit recent hardware and software advances in image acceleration to reduce scanning time and acquire 3D T$_2$ maps within a clinically feasible acquisition time. A respiratory self-navigated 3D acquisition can be used to achieve this goal, as the navigator and slice planning can be avoided, while the sequence performs with 100% acquisition efficiency (compared to $\leq 50\%$ for respiratory-navigator-gated acquisition) (10,11). Furthermore, if a 3D radial trajectory that naturally oversamples the center of k-space is used, motion sensitivity can be minimized (12).

The aim of this study was therefore to develop, implement, and test respiratory self-navigated radial imaging with variable T$_2$Prep for isotropic 3D T$_2$ mapping. To this end, a self-navigated 3D radial T$_2$ mapping pulse sequence was designed. Numerical simulations were used for parameter optimization and to characterize various influences on the T$_2$ fitting process. The accuracy of the T$_2$ mapping was tested in phantoms, its stability was assessed in healthy volunteers and it was preliminarily applied in patients with established cardiovascular disease.

METHODS

Acquisition Protocol

The MRI protocol was based on an undersampled (20% of the Nyquist criterion) electrocardiogram (ECG)-triggered segmented balanced steady-state free precession (bSSFP) 3D radial pulse sequence (repetition time $TR = 2.6$ ms, echo time $TE = 1.33$ ms, radiofrequency (RF) excitation angle 70°, 32 k-space lines per segment, acquisition window 83 ms, no parallel imaging, field of view = (220 mm)^3, matrix=128^3) with a spiral phyllotaxis radial 3D trajectory (12). Briefly, for each k-space segment, the first profile is acquired in the superior-inferior direction, whereas the subsequent radial readouts in the segment are stepped along a spiral 3D pattern, thus causing minimal eddy currents. The following segments are then each rotated by the golden angle (137.51°, as often observed in the leaf arrangement or phyllotaxis in plants) about the superior-inferior axis to assure a homogenous distribution of the readouts in k-space. Using the Fourier transform of the superior-inferior profiles, the respiration-dependent position of the cardiac blood pool is obtained, and respiratory displacement correction is then performed for each k-space segment individually (13). This pulse sequence allows for free-breathing acquisitions with 100% scan efficiency, while ECG triggering every second heartbeat and adiabatic T_2Prep (14) duration $TE_{T2Prep} = 60/30/0$ ms lead to a total acquisition time of ~18 min (3 TE_{T2Prep} × 178 segments × 2 heartbeats/trigger at 60 bpm) with an isotropic spatial resolution of (1.7 mm^3).

Numerical Simulations

Bloch equation (15) simulations of the behavior of the magnetization were performed in MATLAB (The Mathworks, Natick, MA) to determine a fixed relative T_2-fitting offset to correct for T_1 relaxation (5). The T_1 relaxation between the end of the T_2Prep and the middle of the segment will inevitably result in the residual longitudinal magnetization recovery, even for very long TE_{T2Prep}, which will cause an overestimation of T_2. To avoid the need for fitting for both an unknown T_1 and T_2, we previously established that the amount of T_1 relaxation only depends on the pulse sequence parameters (the delay between the T_2Prep and the readout due to ramp-up and navigator pulses, the number of readouts per segment, etc.). We furthermore empirically established that adding an offset η that is constant relative to the steady-state magnetization M_0 compensates for this T_1 relaxation (5):

$$M = M_0 e^{-TE_{T_2Prep}/T_2} + \eta M_0, \qquad [1]$$

where M is the magnetization at a given TE_{T2Prep}. Once the specific offset for the pulse sequence used in this study was established, the dependency of the T_2-fitting process on the heart rate and RF excitation angle was ascertained. For this numerical simulation, "true" in vivo myocardial T_1 and T_2 relaxation times of 1470 and 45 ms were used, respectively (16).

The simulated average magnetization at $TE_{T2Prep} = 0$, 30, and 60 ms were then used in a Monte Carlo simulation to determine the influence of noise on the T_2 fitting process. Random noise from the Rice distribution (17) with a given standard deviation σ_N was added to the three magnetization values and the T_2 value was fitted. This was repeated 10,000 times per standard deviation, and for signal-to-noise ratios ($SNR = M/\sigma_N$) from 1 to 100.

Phantom Experiments

Subsequently, the accuracy of the T_2 fitting was tested in two agar/NiCl$_2$ phantoms (18) that approximated the relaxation times of blood and myocardium. The gold-standard T_2 relaxation time was determined with a spin-echo pulse sequence with eight incremental echo times ($TE = 4$–500 ms, $TR = 5$ s). The T_1 relaxation time was determined with an inversion recovery spin-echo sequence with eight incremental inversion times ($TI = 14$–5000 ms, $TE = 4$ ms, and $TR = 7$ s), and was used in the Bloch equation simulations for the fitting offset specific for the phantoms. Pixel-wise T_2-mapping was then performed in MATLAB. A 5-pixel-diameter Gaussian filter was then applied to smooth the T_2 maps.

Healthy Volunteer Studies

The in-vivo robustness of the T_2 determination in the presence of cardiac and respiratory motion was then tested in 10 healthy adult volunteers (age 27 ± 3 years, weight 73 ± 14 kg, seven men) on a clinical 3T system (Magnetom Skyra, Siemens, Erlangen, Germany) with a 30-channel phased-array coil. Permission was obtained from the Institutional Review Board and all subjects provided written informed consent prior to the scans. After a localizer pulse sequence and a cine sequence to determine the most quiescent diastolic rest period, localized cardiac shimming (19) was applied. The imaged volume for T_2 mapping encompassed the entire heart as visualized on the localizer scans and was centered at a left-ventricular level. In the dataset with $TE_{T2Prep} = 60$ ms of all volunteers, the myocardial SNR in the region with the lowest signal intensity (visually determined) was measured to estimate the effect of low SNR on the T_2 quantification as determined through the Monte Carlo simulations. The 3D datasets obtained with different TE_{T2Prep} were registered using 3D affine registration (20).

The resultant datasets were multiplanar reformatted in a short-axis orientation, and the AHA-standard 16-sector segmentation (21) of a single basal, mid-ventricular, and apical slice of the left ventricle (LV) was used to assess the homogeneity of the T_2 values. The borders of the myocardium were avoided in the segmentation to account for minor misregistrations of the source images. Paired Student's t-tests with Bonferroni correction for multiple comparisons were applied to test for T_2 differences between segments and slices. The entire LV was then segmented in MATLAB as a contour in the middle of the myocardium of each slice to construct a 3D surface to visually assess the overall T_2 homogeneity.

Preliminary Patient Studies

To translate this new technology to the patient setting, the described pulse sequence was applied for the detection of edema in three patients with established cardiovascular
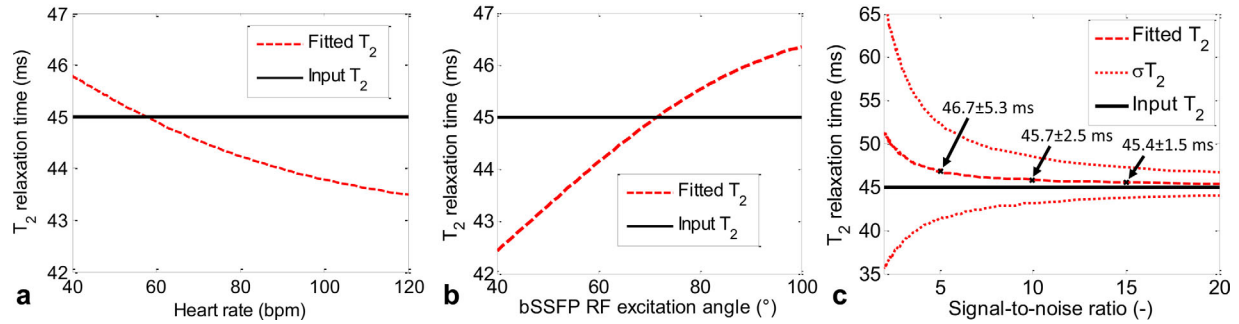
FIG. 1. Numerical simulations demonstrate the robustness of the 3D T$_2$ mapping technique. **a:** Bloch equation simulation illustrating that the dependence of the T$_2$ fit of the magnetization on the heart rate due to the influence of varying T$_1$ relaxation on the magnetization is relatively low. It varies between 43 and 46 ms, a variation of 3%, while the "true" input T$_2$ was 45 ms. **b:** A similar simulation for variation in the RF excitation angle that might be caused by B$_1$ inhomogeneity demonstrates that an overestimation or underestimation of the angle also causes an overestimation or underestimation of the estimated T$_2$ value in a relatively narrow range. **c:** Monte Carlo simulations illustrate the dependence of the T$_2$ fitting accuracy and its standard deviation σT$_2$ on the level of Rician noise. At the lowest myocardial SNR observed in vivo (SNR = 10), the input T$_2$ value is overestimated by 0.7 ms. [Color figure can be viewed in the online issue, which is available at wileyonlinelibrary.com.]

disease: a patient with a subacute myocardial infarction 6 days prior to MRI (age 75 years, weight 85 kg, male, infarction confirmed by elevated creatine kinase-MB) and revascularization of his proximal left coronary circumflex, a patient with acute myocarditis (age 24 years, weight 84 kg, male), and a cardiac allograft patient (age 61 years, weight 63 kg, male) with no detectable graft rejection (rejection grade 0R) (22) as established by endomyocardial biopsy, but a high heart rate of 90 bpm. In these patients, the LV myocardium was segmented from the 3D T$_2$ maps as described for the volunteers, and regions with elevated T$_2$ were defined as those having an average T$_2$ value that was at least three standard deviations above their remote myocardial counterpart T$_2$. In the patients with myocarditis and graft rejection, variable-T$_2$Prep navigator-gated gradient-echo-based radial 2D T$_2$ maps (TE$_{T2Prep}$ = 0/30/60 ms, TR/TE = 7.6/2.8 ms, RF excitation angle 15°, 21 k-space lines per heartbeat, three heartbeats trigger interval, voxel size 1.25 × 1.25 × 5 mm^3) (5) were additionally acquired at a basal, mid-ventricular, and apical short-axis level for comparison.

RESULTS

Accuracy and Homogeneity in Simulations and Phantoms

The Bloch equation simulations of the pulse sequence demonstrated that, at a heart rate of 60 bpm, the standard exponential decay overestimates the input T$_2$ value by 11–14% in the physiological range at 3T (35–65 ms). The input T$_2$ value of 45 ms was most accurately fitted from the magnetization M with the following empirical equation:

$$M = M_0 e^{-\text{TE}_{T2Prep}/T_2} + 0.08 M_0. \qquad [2]$$

When using this equation, the fitted T$_2$ had only a ~5% variation over the common range of expected heart rates, while the variation in RF excitation angle caused a ~9% variation over the entire range (Fig. 1a,b). The Monte Carlo simulations furthermore demonstrated that at very low SNR, the Rician noise causes the T$_2$ value to be overestimated (Fig. 1c).

The 3D T$_2$ maps of the phantoms demonstrated high spatial homogeneity and fitting accuracy in all dimensions in the compartment that mimics the myocardium (Fig. 2a,b). At 35.4 ± 1.7 ms versus the gold standard 35.7 ± 0.8 ms, the average T$_2$ value with the 3D sequence matched the gold-standard T$_2$ value within 1% (Fig. 2c), suggesting a high accuracy of the 3D pulse sequence for T$_2$ quantification in this T$_2$ range.

Robustness in Volunteers

The volunteer study (Fig. 3) confirmed the duration of the protocol at 18.2 ± 1.7 min and resulted in an average myocardial T$_2$ value of 40.5 ± 3.3 ms. The T$_2$-prepared source images were of high quality (Fig. 3a–d), and the lowest SNR in the myocardium over the volunteers was 11.4 ± 1.5. The isotropic resolution allowed for easy reformatting in any desired orientation (Fig. 3e,f). The segment analysis in the volunteers (Fig. 3g) showed a slight decrease in T$_2$ from the base to the apex (43.3 ± 2.0 ms vs. 37.4 ± 2.4 ms, $P = 0.002$), while neither was statistically significant vs. the mid-ventricle at 40.6 ± 2.4 ms. Similarly, a slight decrease in T$_2$ value from the inferior toward the anterior segment was observed (42.4 ± 5.3 ms vs. 37.2 ± 4.9 ms, $P < 0.001$). 3D segmentation and rendering allowed for a quick overview of the global T$_2$ values (Fig. 3h).

Edema Detection in Patients

In the LV of the myocardial infarction patient, a large region of significantly elevated T$_2$ (60.4 ± 9.1 ms vs. 41.0 ± 4.5 ms in a remote segment: a 47% increase in T$_2$) was identified in the inferior and lateral myocardium (Fig. 4a,b), consistent with the finding of a luminal narrowing in the proximal left coronary circumflex by X-ray coronary angiography. In the patient with myocarditis (Fig. 4c,d), a regional elevation (47.3 ± 5.1 ms vs. 36.3 ± 3.7 ms in the healthy remote area) was observed in the basal lateral wall, which was confirmed on the 2D T$_2$ maps (50.3 ± 6.2 ms vs. 36.5 ± 3.1 ms). However, as this T$_2$ elevation was not transmural, the region appeared smaller in the 3D
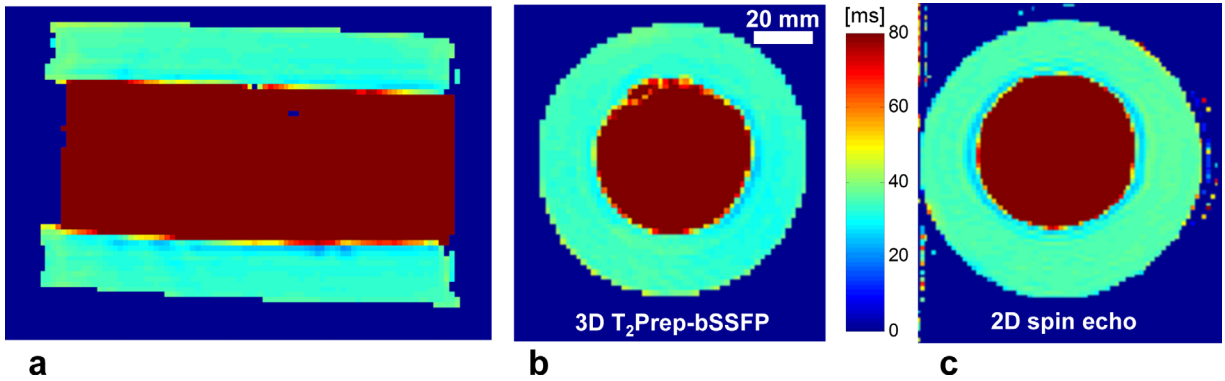
FIG. 2. Phantom validations demonstrate the accuracy and homogeneity of the 3D T_2 mapping technique. **a, b:** Perpendicular slices through a 3D T_2 map of a cylindrical phantom that approximates arterial blood (red) and myocardium (green) obtained with the 3D technique. At 35.4 ± 1.7 ms, the "myocardial" T_2 value is homogeneous throughout both cross sections of the compartment with myocardial tissue properties (T_1 and T_2 relaxation times). As the display range was chosen to illustrate variations in the T_2 value of the outer compartment (simulated myocardium), the T_2 of the inner compartment (simulated blood with $T_2 \sim 150$ ms) falls outside of the display range. **c:** T_2 map of the same phantom obtained with the gold-standard 2D spin-echo. The T_2 values of the "myocardium" compartment are also highly homogeneous and at 35.7 ± 0.8 ms very similar to the 3D T_2 map values. Dark-blue regions were below the signal threshold and were not mapped.

mid-myocardial segmentation than it does in the 2D T_2 map (Fig. 4c,d,g). The graft transplantation patient demonstrated a homogeneous T_2 distribution both in the 3D (38.9 ± 4.7 ms) and 2D (37.7 ± 2.7 ms) T_2 maps, which was consistent with the lack of rejection observed through endomyocardial biopsy (Fig. 4e,f,h).

DISCUSSION

Self-navigated 3D T_2 mapping with an isotropic 1.7-mm spatial resolution was characterized in numerical simulations and phantom experiments, and was successfully applied in both healthy volunteers and preliminarily in patients with established cardiovascular disease. No
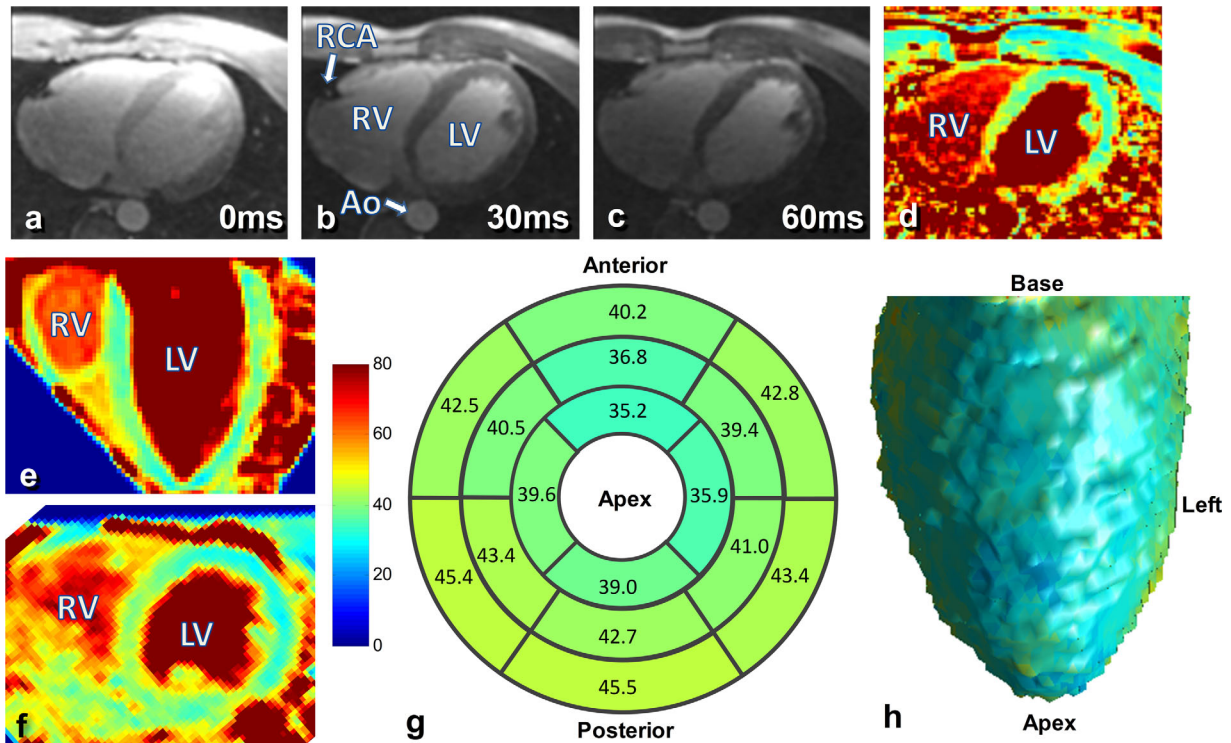

FIG. 3. 3D T_2 mapping in healthy volunteers demonstrates a homogeneous T_2 distribution. **a–d:** Three axial source images with different T_2Prep times and their corresponding T_2 map. Despite the relatively low resolution, fine details like the right coronary artery can be identified. **e, f:** A long-axis and a mid-ventricular short-axis slice through the LV show homogenous T_2 values throughout the myocardium. **g:** AHA standard segmentation of the 3D T_2 maps demonstrates that the average T_2 value distribution is homogeneous in all 10 subjects, with small gradients in both the anterior-inferior and base-apex directions. **h:** A 3D volume rendering of the LV of a healthy volunteer as seen from the anterior further illustrates the homogeneous 3D distribution.
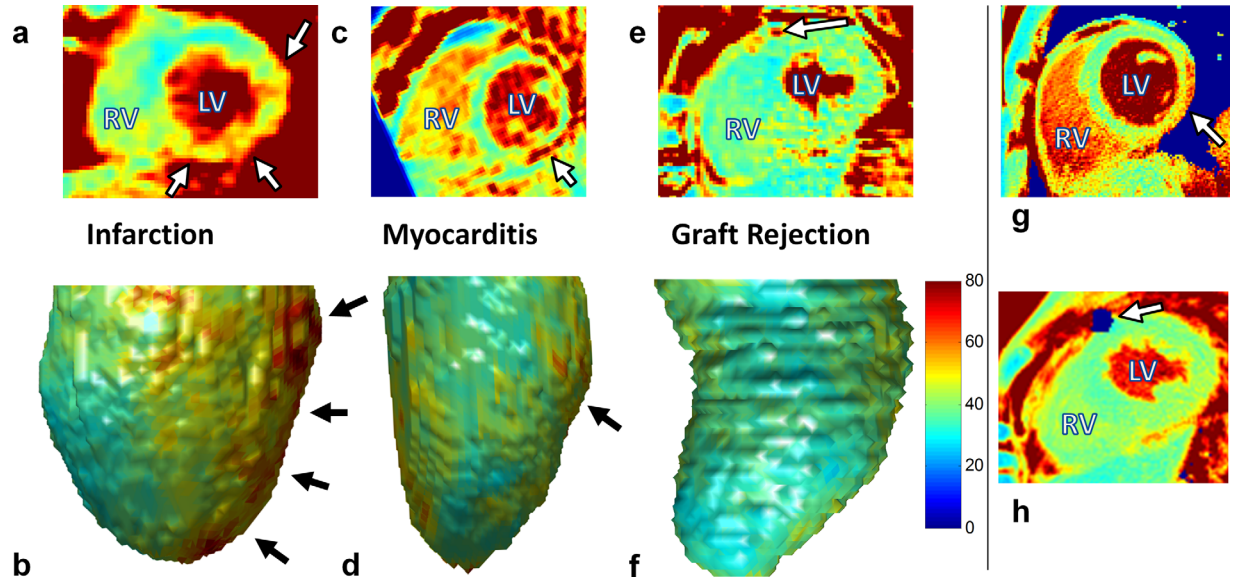
FIG. 4. Short-axis slices and 3D volume renderings of the 3D T$_2$ maps in three patients with established cardiovascular disease. **a, b:** A patient with a subacute myocardial infarction as confirmed through X-ray angiography. A region with significantly elevated T$_2$ can be clearly identified (arrows). **c, d:** A patient with myocarditis that was established through prior clinical MRI. Several small regions of T$_2$ elevation can be discerned (arrows). **e, f:** A patient with a cardiac graft and no rejection as seen in endomyocardial biopsy also demonstrates the absence of subendocardial elevated T$_2$ values, although a small patch with elevated T$_2$ can be observed at the anterior epicardium (arrow). This was later confirmed to be a stent. **g:** A region of elevated T$_2$ can be observed in a control 2D T$_2$ map at the same level as (c). However, the region is mostly epicardial and not transmural, which causes it to appear smaller in the 3D subendocardial segmentation. **h:** A control 2D T$_2$ map at the same level as (e). The myocardium also does not show any T$_2$ elevation, while the blue patch here is a nonmapped signal void, which was confirmed to be the same stent as in (e).

navigator placement or double-oblique anatomical slice orientations is necessary, which allows for minimal planning time and reduced user-interaction in-between scans. Moreover, the isotropic spatial resolution and whole heart coverage enable retrospective multiplanar reformatting in any user-selected slice orientation and anatomical level of the heart.

Numerical Simulations Confirmed by Phantom Studies with Gold Standard

The Bloch equation simulations demonstrated that there is a non-zero residual to which the magnetization decays. This residual is attributable to T$_1$ recovery after the T$_2$Prep and during the signal readout train. In fact, this is consistent with the residual observed for a 2D radial T$_2$-mapping approach implemented at 3T (5). We chose to approximate this residual with a fixed offset, as the analytical solution would require the input of the T$_1$ value, which is not known a priori in vivo. However, in practice, if T$_2$ maps were acquired together with T$_1$ mapping data, such an analytical solution could perhaps be implemented and tested. The simulations furthermore demonstrated that the method is robust against heart rate variations and B$_1$ inhomogeneities. The Monte Carlo simulations demonstrated that at low SNR, the noise will cause an overestimation of the T$_2$ value, which should coincide with a high standard deviation.

The accuracy of the Bloch equation simulations was confirmed in the phantom study where the values obtained with the proposed 3D T$_2$ mapping technique were consistent with those from the gold-standard spin-echo T$_2$ maps. The high spatial homogeneity and low

standard deviation of the T$_2$ values of ~5% further demonstrated the robustness of the pulse sequence in vitro.

In Vivo Application Demonstrates Precision and Robustness of T$_2$ Mapping

The T$_2$ values in the healthy volunteers were consistent with those previously reported at 3T yet obtained with a 2D technique, and have a similar standard deviation of ~8% (5). Gradients in measured T$_2$ values were observed in both the base to apex direction and around the circumference from the anterior to the inferior short-axis segments. As the anterior and posterior parts of the heart are positioned differently within the RF-excitation body coil, it is possible that there is a residual decreasing gradient of effective RF excitation angles from the anterior to the posterior. As calculated with the Bloch equation simulations (Fig. 1b), such a gradient in effective RF excitation angle might, therefore, result in a minor gradient of T$_2$ values in the anterior-inferior direction. Future studies could, for example, try to correct for this effect by incorporating maps of the effective RF excitation angle. Simultaneously, different distances from the receive coils might result in decreased SNR in the inferior segments, which could in turn result in a T$_2$ overestimation as demonstrated with the Monte Carlo simulations. However, given that the lowest myocardial SNR of the T$_2$Prep = 60 ms images is on the order of ~10, this should account for only about 1 ms of overestimation. Differences in instantaneous regional myocardial perfusion (and thus oxygenation) between the base and apex may furthermore lead to the observed variations in the apex-base direction. Other studies (4,23) also observed variations in the apex-

base directions. However, as these studies used 2D Cartesian breath-held T_2 mapping, a direct comparison may not be straightforward.

All three patient studies demonstrated homogeneous and normal T_2 values in healthy regions and significantly elevated T_2 values in regions of suspected edema, while the edematous T_2 in the patient with the preceding myocardial infarction agreed with previously published values (5). However, the patient with myocarditis demonstrated that a region of nontransmural T_2 elevation as observed on 2D T_2 mapping is not always entirely detected when the 3D images are interpreted, mainly due to the proximity of the elevated T_2 values to the lung tissue, which has a noisy high apparent T_2 value.

Study Limitations

Although this 3D T_2 mapping approach appears robust in the volunteers, its performance should also be thoroughly evaluated in patients. Another potential limitation of self-navigated isotropic 3D cardiac T_2 mapping is its duration. A shortening of the scan time could, for example, be achieved by lowering the number of acquired radial lines in k-space, acquiring more lines per heartbeat, waiting fewer heartbeats between acquisitions, partial acquisition schemes, such as k-space weighted image contrast (KWIC) (24), the use of compressed sensing, or saturation-recovery prepulses instead of three heartbeats of waiting time (25). However, the effects of all such scan time shortening techniques on the performance of T_2 mapping remain to be more thoroughly investigated.

CONCLUSIONS

We successfully implemented, tested, and characterized a spatially isotropic self-navigated free-breathing 3D T_2 mapping technique at 3T. The technique preliminarily allows for the 3D characterization of edema in established cardiovascular disease in less than 20 min.

REFERENCES

1. Friedrich MG. Myocardial edema—a new clinical entity? Nat Rev Cardiol 2010;7:292–296.
2. Manka R, Kozerke S, Rutz AK, Stoeck CT, Boesiger P, Schwitter J. A CMR study of the effects of tissue edema and necrosis on left ventricular dyssynchrony in acute myocardial infarction: implications for cardiac resynchronization therapy. J Cardiovasc Magn Reson 2012;14:47.
3. Huang TY, Liu YJ, Stemmer A, Poncelet BP. T2 measurement of the human myocardium using a T2-prepared transient-state TrueFISP sequence. Magn Reson Med 2007;57:960–966.
4. Giri S, Chung YC, Merchant A, Mihai G, Rajagopalan S, Raman SV, Simonetti OP. T2 quantification for improved detection of myocardial edema. J Cardiovasc Magn Reson 2009;11:56.
5. van Heeswijk RB, Feliciano H, Bongard C, Bonanno G, Coppo S, Lauriers N, Locca D, Schwitter J, Stuber M. Free-breathing 3 T magnetic resonance T(2)-mapping of the heart. JACC Cardiovasc Imaging 2012;5:1231–1239.
6. Thavendiranathan P, Walls M, Giri S, Verhaert D, Rajagopalan S, Moore S, Simonetti OP, Raman SV. Improved detection of myocardial involvement in acute inflammatory cardiomyopathies using t2 mapping. Circ Cardiovasc Imaging 2012;5:102–110.
7. Markl M, Rustogi R, Galizia M, Goyal A, Collins J, Usman A, Jung B, Foell D, Carr J. Myocardial T2-mapping and velocity mapping: changes in regional left ventricular structure and function after heart transplantation. Magn Reson Med 2013;70:517–526.
8. Usman AA, Taimen K, Wasielewski M, et al. Cardiac magnetic resonance T2 mapping in the monitoring and follow-up of acute cardiac transplant rejection: a pilot study. Circ Cardiovasc Imaging 2012;5:782–790.
9. Gharib AM, Abd-Elmoniem KZ, Herzka DA, Ho VB, Locklin J, Tzatha E, Stuber M, Pettigrew RI. Optimization of coronary whole-heart MRA free-breathing technique at 3 Tesla. Magn Reson Imaging 2011;29:1125–1130.
10. Stehning C, Bornert P, Nehrke K, Eggers H, Stuber M. Free-breathing whole-heart coronary MRA with 3D radial SSFP and self-navigated image reconstruction. Magn Reson Med 2005;54:476–480.
11. Piccini D, Monney P, Sierro C, et al. Respiratory self-navigated post-contrast whole-heart coronary mr angiography: initial experience in patients. Radiology 2014;270:378–386.
12. Piccini D, Littmann A, Nielles-Vallespin S, Zenge MO. Spiral phyllotaxis: the natural way to construct a 3D radial trajectory in MRI. Magn Reson Med 2011;66:1049–1056.
13. Piccini D, Littmann A, Nielles-Vallespin S, Zenge MO. Respiratory self-navigation for whole-heart bright-blood coronary MRI: methods for robust isolation and automatic segmentation of the blood pool. Magn Reson Med 2012;68:571–579.
14. Nezafat R, Stuber M, Ouwerkerk R, Gharib AM, Desai MY, Pettigrew RI. B1-insensitive T2 preparation for improved coronary magnetic resonance angiography at 3 T. Magn Reson Med 2006;55:858–864.
15. Bloch F. Nuclear Induction. Phys Rev 1946;70:460–474.
16. Stanisz GJ, Odrobina EE, Pun J, Escaravage M, Graham SJ, Bronskill MJ, Henkelman RM. T1, T2 relaxation and magnetization transfer in tissue at 3T. Magn Reson Med 2005;54:507–512.
17. Gudbjartsson H, Patz S. The Rician distribution of noisy MRI data. Magn Reson Med 1995;34:910–914.
18. Kraft KA, Fatouros PP, Clarke GD, Kishore PR. An MRI phantom material for quantitative relaxometry. Magn Reson Med 1987;5:555–562.
19. Greiser A, Weber O, Deshpande V, Mueller E. Improved cardiac shimming in a clinical setting by multi-frame fieldmap acquisition and automatic ROI extension. In SCMR 10 Proceedings, Rome, Italy, 2007. p. 373.
20. Studholme C, Hill DL, Hawkes DJ. Automated 3-D registration of MR and CT images of the head. Med Image Anal 1996;1:163–175.
21. Cerqueira MD, Weissman NJ, Dilsizian V, Jacobs AK, Kaul S, Laskey WK, Pennell DJ, Rumberger JA, Ryan T, Verani MS. Standardized myocardial segmentation and nomenclature for tomographic imaging of the heart. Circulation 2002;105:539–542.
22. Rosenthal D, Chrisant MR, Edens E, et al. International society for heart and lung transplantation: practice guidelines for management of heart failure in children. J Heart Lung Transplant 2004;23:1313–1333.
23. von Knobelsdorff-Brenkenhoff F, Prothmann M, Dieringer MA, Wassmuth R, Greiser A, Schwenke C, Niendorf T, Schulz-Menger J. Myocardial T1 and T2 mapping at 3 T: reference values, influencing factors and implications. J Cardiovasc Magn Reson 2013;15:53.
24. Song HK, Dougherty L. k-space weighted image contrast (KWIC) for contrast manipulation in projection reconstruction MRI. Magn Reson Med 2000;44:825–832.
25. Ding H, Xu D, Zviman MM, Sena-Weltin V, Amado L, Nazarian S, Halperin H, McVeigh ER, Herzka DA. High spatial resolution free breathing 3D T2 mapping for edema detection in radio frequency ablation. In Proceedings of the 19th Annual Meeting of ISMRM, Montreal, Canada, 2011. p. 23.